International Journal of Technology 13(4) 803-815 (2022)
Received January 2022 / Revised February 2022 / Accepted March 2022

International Journal of Technology

http://ijtech.eng.ui.ac.id

Evaluation of Piezoaeroelastic Energy Harvesting Potential of a Jet Transport Aircraft Wing with Multiphase Composite using Iterative Finite Element Method

Mahesa Akbar[1*], Mileniawan Januar Ramadhani[1], Mohammad Arif Izzuddin[1], Leonardo Gunawan[1], Rianto Adhy Sasongko[1], Muhammad Kusni[1], Jose Luis Curiel-Sosa[2]

[1]*Faculty of Mechanical and Aerospace Engineering, Institut Teknologi Bandung, Jalan Ganesa 10, Bandung 40132, Indonesia*
[2]*Department of Mechanical Engineering, The University of Sheffield, Mappin Street, Sheffield S13JD, United Kingdom*

Abstract. This paper presents new insight on the potential of piezoaeroelastic energy harvesting on the transport aircraft wing structure. A novel numerical investigation is conducted in the present study. An advanced iterative finite element method (FEM) is applied to estimate the amount of harvested energy. Currently, FEM-based commercial software has a limited application on piezoelectric structures, i.e., actuator and sensor. The iterative FEM algorithm extends the commercial software implementation for the energy harvesting analysis. The multidisciplinary issue of the aeroelastic phenomenon and piezoelectric energy harvesting is evaluated in the present case. Likewise, interestingly, stress and failure analysis of a lifting surface with an active energy harvesting component could be enabled. Implementation of a wing with an embedded piezoelectric layer is concerned. A cruise flight condition and gust disturbance are evaluated. The analysis concerning the occurrence of gust also provides a more realistic insight into the power harvested during a flight operation.

Keywords: Aircraft wing; Energy harvesting; Gust load; Iterative FEM; Piezoaeroelastic

1. Introduction

Many researchers have been attracted by multifunctional material systems in the past few decades (Ferreira et al., 2016; Sairajan et al., 2016). The article by Christodolou and Venables (Christodoulou & Venables, 2003) is one of the earliest publications on this subject. They highlighted the combination of structural functions, i.e., load-bearing, with power generation, the so-called structural-power system.

In the new and renewable energy topic, many studies and technologies rely on ambient sources, i.e., wind, thermal, and solar (Krasniqi et al., 2022; Brazovskaia & Gutman, 2021; Guenther, 2018; Hafizh et al., 2018; Selvan & Ali, 2016; Thomas et al., 2006). In terms of structural-power systems, piezoelectric energy harvesting has been one of the promising subjects (Anton & Sodano, 2007). In a lifting structure, i.e., aircraft, the vibration exerted by the fluid-structure interaction is one of the sources to harvest the energy (Abdelkefi, 2016; Li et al., 2016; Rostami & Armandei, 2017).

*Corresponding author's email: mahesa_akbar@itb.ac.id, Tel.: +62222504243, Fax.:+622222505425
doi: 10.14716/ijtech.v13i4.5468

Anton and Inman (2008) pioneered the experimental study on piezoelectric energy harvesting from aircraft structures. They have successfully flight-tested a remote control aircraft with active piezoelectric energy harvesters attached to the wing spars and fuselage. Numerous mathematical and computational methods have also been studied.

One of the first mathematical models on this topic was developed by Erturk et al. (2010). They coined the term piezoaeroelastic energy harvesting, which defines the energy harvesting from aeroelastic vibration of the piezoelectric-based structure. Their proposed mathematical model concerns a flutter-based energy harvesting from 2 Degree-of-Freedoms (DoF) airfoil. They have also performed a wind tunnel test for validation.

Following the success of the airfoil model, higher fidelity computational models have been developed. Planar lifting structure models were proposed for time-domain (De-Marqui et al., 2010) and frequency-domain (De-Marqui al., 2011) problems. The models utilized the electromechanical shell element (De-Marqui et al., 2009).

Although a significant number of studies involved with experimental fluid-structure interaction tests, there is a lack of investigation concerning more functional aerodynamic conditions (Abdelkefi, 2016). Most of studies focused on instability and resonance conditions, i.e., flutter, galloping, and vortex induced vibration (Rostami & Armandei, 2017). However, an instability or resonance phenomenon could lead to a structural failure.

To the authors' knowledge, only a few publications discussed the development of models concerning piezoaeroelastic energy harvesting from operational aerodynamic conditions. The investigation on energy harvesting from discrete gust loads, i.e., 1-cosine and square gusts, were discussed by Xiang et al. (2015), Bruni et al. (2017), Cheng et al. (2019), Saporito and Da-Ronch (2020). Tsushima and Su (2016) presented a computational model to evaluate turbulence conditions. They extended their model in combination with an active control system (Tsushima & Su, 2017).

Akbar and Curiel-Sosa investigated the cruise flight condition of a civil jet transport aircraft in (Akbar & Curiel-Sosa, 2016). Akbar and Curiel-Sosa (2018) discussed the extension of this study in their article. By implementing multiphase piezoelectric composites, it was claimed up to 40 kW of power can be harvested and may be used as an alternative for reducing the fuel consumption (Akbar & Curiel-Sosa, 2018). However, the computational tools were limited on a harmonic bending motion. Furthermore, the studies neglected the two-ways coupling between the aerodynamic loads and the structural deformation. Therefore, one of the research gaps is on the investigation of a more realistic load case, i.e., involved a more sophisticated interaction concerning aerodynamics, structures and electrical domains. In the present work, thus, the main problem statement is how to evaluate a more realistic load case using numerical methods.

A so-called iterative finite element method (FEM), was proposed by Akbar and Curiel-Sosa (2019). The iterative FEM was developed to use FEM-based commercial software with augmentation of a simple computational program to evaluate electromechanical coupling of energy harvesting cases. This method has been validated and proven to estimate the energy harvested from lifting structures, i.e., bimorph plate and UAV wing.

In the present work, for the first time, the iterative FEM is utilized to investigate the energy harvesting potential of a jet transport aircraft wing. Hence, enabling the evaluation for a more practical flight condition, i.e., aeroelastic condition concerning a cruise flight and discrete 1-cosine gust disturbance. Various gust velocities considering the occurrence probability are concerned. The following sections present the fundamental of the iterative FEM and the results of the aircraft wing numerical investigation.

2. Methods

The present work uses the constitutive forms of piezoelectric material based on the IEEE standard. The submatrices of an electromechanical constitutive matrix, **Σ**, is expressed in Equation (1). The stress-charge transformation into strain-charge form is depicted in Equation (2).

$$\boldsymbol{\Sigma} = \begin{bmatrix} \mathbf{C} & -\mathbf{e}^t \\ (6\times 6) & (6\times 3) \\ \mathbf{e} & \boldsymbol{\varepsilon}^{\boldsymbol{S}} \\ (3\times 6) & (3\times 3) \end{bmatrix} \tag{1}$$

S and **C** are the compliance and the elasticity matrices, respectively. **e** and **d** are the coupling constants. Due to orthotropic properties, symmetries are applied, i.e., $d_{31} = d_{32}$, $C_{11} = C_{22}$, etc. The permittivity in the forms of strain-charge and stress-charge are denoted by $\boldsymbol{\varepsilon}^{\boldsymbol{T}}$ and $\boldsymbol{\varepsilon}^{\boldsymbol{S}}$.

$$\begin{aligned} \mathbf{C} &= \mathbf{S}^{-1} \\ \mathbf{e} &= \mathbf{d}\mathbf{S}^{-1} \\ \boldsymbol{\varepsilon}^{\boldsymbol{S}} &= \boldsymbol{\varepsilon}^{\boldsymbol{T}} - \mathbf{d}\mathbf{S}^{-1}\mathbf{d}^t \end{aligned} \tag{2}$$

In a finite element-based problem, the governing equations of piezoelectric finite elements has been well established for actuation case. Akbar and Curiel-Sosa modified the equation of the actuation problem to accommodate the energy harvesting effect (Akbar & Curiel-Sosa, 2019). In the actuation system, the piezoelectric material receives an amount of electrical input to be converted into a mechanical response, i.e., structural deformation. However, as an energy harvester, the piezoelectric material generates electrical energy from its own deformation.

An illustration of a fundamental piezoelectric-based energy harvesting structure is shown in Figure 1. The harvestings structure made of piezoelectric material is layered on a host structure. The host structure is not contributed directly to any electrical response of the system. However, it is contributed to the mechanical deformation which further influences the electrical response. In Figure 1, an example of a distributed force as mechanical loading and resistance as electrical load. The 1,2,3 directions are correlated with the electromechanical constitutive tensor as expressed in Equation (1).

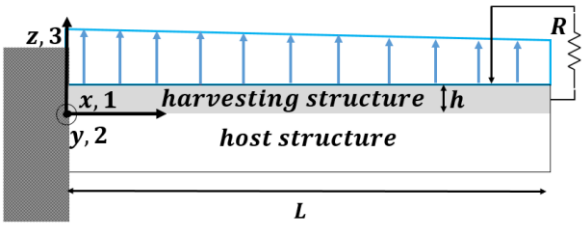

Figure 1 A typical piezoelectric-based energy harvesting structure

The modified equations for piezoelectric energy harvesting based on (Akbar & Curiel-Sosa, 2019) are written as:

$$\mathbf{M}\mathrm{U} + \mathbf{G}\dot{\mathrm{U}} + \mathbf{K}_{\mathrm{uu}}\mathrm{U} = \mathbf{F} - \mathbf{K}^*_{\mathrm{uv}}V \tag{3}$$

and

$$-\mathbf{K}^*_{\mathrm{vu}}\dot{\mathrm{U}} + K_{vv}\dot{V} + \frac{V}{R} = 0 \tag{4}$$

Both Equations (3) and (4) incorporate the mechanical DoF, n_m, depending on the size and type of the elements. The accent on the variables represented by dot, $(\dot{\ })$, or double dots, $(\ddot{\ })$, depict the first or the second derivative concerning time. The vectors $\mathbf{U}$ $(n_m \times 1)$ and $\mathbf{F}$ $(n_m \times 1)$, respectively, are the global displacement and the mechanical force. $\mathbf{M}$ $(n_m \times n_m)$ and $\mathbf{G}$ $(n_m \times n_m)$ represent the worldwide mass and mechanical damping matrices. The global stiffness matrix, $\boldsymbol{K_{uu}}(n_m \times n_m)$, is associated with the elasticity matrix in Equation (1).

The scalar voltage term, V, multiplied with the electromechanical coupling vector $\boldsymbol{K^*_{vu}}$ is equivalent to the forcing vector. The coupling vector $\boldsymbol{K^*_{vu}} = \boldsymbol{K^*_{uv}}^{\boldsymbol{T}}$ and $\boldsymbol{K_{vv}}$ is the capacitance of the piezoelectric layer. These vectors are associated with the coupling constant and the permittivity in Equation (2). The resistance load, R, is applied to complete the electrical circuit.

The piezoelectric layer is poled in the thickness direction. The layer is assumed to be very thin, and a continuous electrode is used on the whole surfaces. Thus, all elements of the piezoelectric layer can be assumed to generate the same voltage. Hence, the voltage V is a scalar applied to all the piezoelectric nodes (De-Marqui et al., 2009).

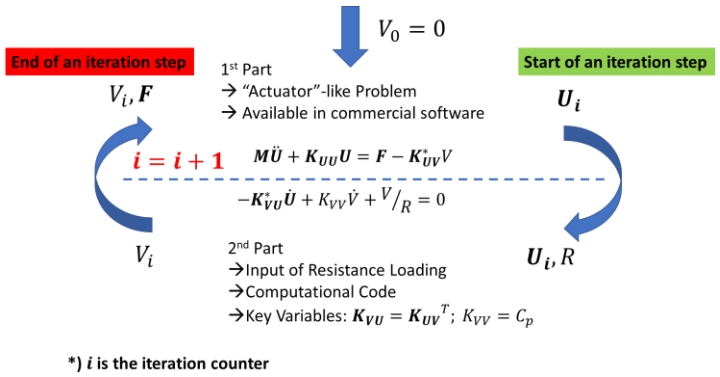

Figure 2 Algorithm of the Iterative FEM

A general procedure of the iterative FEM is illustrated in Figure 2. The idea of the iterative FEM is the iterative processes applied to obtain the solutions of Equations (3) and (4). On each iteration, the structural responses and the voltage will be updated until the values between two consecutive iterations converge. Akbar and Curiel-Sosa suggested to start the iterative procedure assuming no voltage is applied, $V = 0$. For a more detailed explanation and algorithm, the reader is referred to Akbar and Curiel-Sosa (2019).

3. Results and Discussion

3.1. Wing Configuration and Aeroelastic Analysis

The investigation of the harvested energy on a jet transport aircraft wing is described in this section. The typical 1-cosine gust is applied as the excitation load acting on the wing. The airplane wingbox model utilized in the current work depends on the setup in (Akbar & Curiel-Sosa, 2016). Be that as it may, a few adjustments are used in this work, to have a more practical design like those in an average long-range flight airplane, i.e., Boeing 737-800. A 300 sweptback change in view of an ordinary stream airplane wing in (Ainsworth et al., 2010) is applied. The wing arrangement including the structural and aerodynamic models from the top view is displayed in Figure 3.

Figure 3 depicts the wingbox structural parts modeled as shell elements. The ribs and the spars are 7.04 mm in thickness and for the skins are 6.09 inches. The fixed

(cantilevered) boundary condition is applied on the root. Initially, the wingbox materials are Aluminium Alloy, Al-2219, with a density 2840 kg/m^3 and Young's modulus 73.1 GPa.

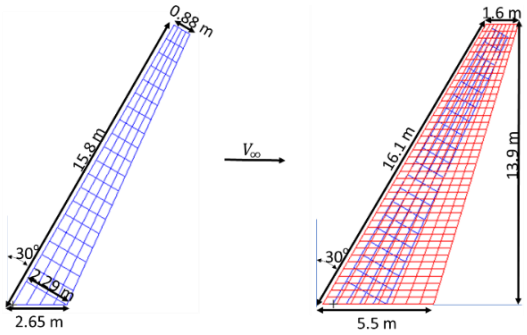

Figure 3 Aircraft wingbox arrangement (top perspective): wingbox structural model (left), wingbox and aerodynamic panels (right)

In the current analysis, the upper skin is replaced by a pure piezoelectric material, PZT-5A. Furthermore, in Section 3.2, the result of the multiphase composite implementation is discussed. Unidirectional laminated utilising shell elements is used to model the upper skin part which piezoelectric 1-direction lies across the midchord span.

The mode shapes and its natural frequency of the wingbox can be seen in Figure 4 which the natural frequency of the 1st bending, the 2nd bending and the 1st torsion modes are 1.72 Hz, 7.36 Hz and 23.47 Hz, respectively. Following the fundamental ways, i.e., bending and torsion, the higher methods are the mixed of two or more basic ways, i.e., mix bending and torsion mode at 31.50 Hz. In the present work, flutter analysis is conducted to investigate the frequency and damping ratio changes to the airspeed.

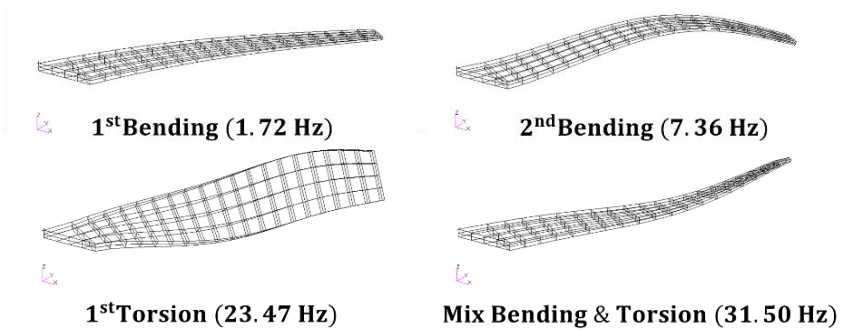

Figure 4 Mode shapes the aircraft wingbox

The red frame in Figure 3 shows the surface of the wing divided into a series of aerodynamic panels. Aircraft wings are represented by aerodynamic panels that cover a much larger surface area than structural elements. Ten modes are included in the analysis to compensate for the effects of high-frequency's modes. Flutter analysis is performed at a cruising altitude of 10000 m above sea level, at subsonic and low supersonic regimes. The Doublet Lattice Method (DLM) aerodynamic model is used in the subsonic range (up to Mach 0.8) and Zona 51 Method is applied for the low supersonic regime (Mach 1.2 – 2.0). For the transonic regime, a much more complex phenomenon should be evaluated by a higher fidelity transient aerodynamic model, i.e., RANS. Thus, in the present work, for flutter analysis, only subsonic and low supersonic regime is observed. Figure 5 shows a flutter summary in the form of V-g and V-f graphs.

In both Figures 5a and 5b, it can be observed that neither damping nor frequency show any signs of instability. No flutter occurs in the subsonic nor supersonic regime. The only

indication towards instability behavior is the frequency of the 1st torsion starts to decrease, moving closer to the 2nd bending. If this trend continues and both modes coalescence; thus, coupling occurs and instability could happen.

However, it is understandable that if the cruising speed of a typical medium-range jet transport aircraft is Mach 0.8 (240 m/s), the critical flutter speed will exceed 300 m/s (Mach 1). Moreover, as can be seen in Figure 5, there is a possibility that flutter will occur outside the subsonic range, either at supersonic speed or within transonic regime. Thus, it is not practical to observe above the subsonic regime, as this typical aircraft will not operate above those limits.

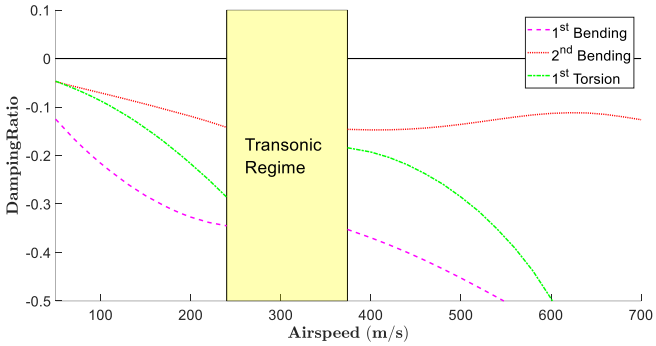

(a)

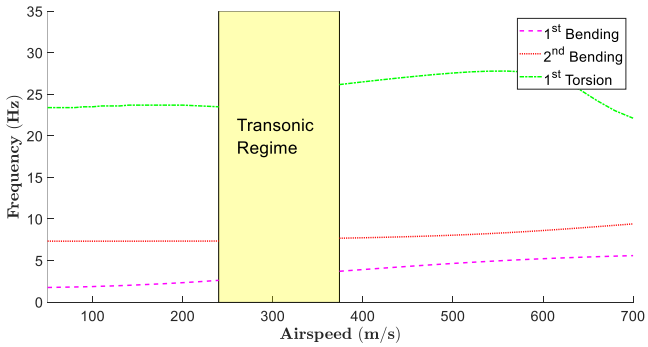

(b)

Figure 5 The result of flutter analysis of the wingbox: (a) Airspeed vs damping ratio (*V-g*), and (b) airspeed vs frequency (*V-f*) graphs of the aircraft wingbox

3.2. Analysis of Piezoaeroelastic Energy Harvesting

The aeroelastic situation concerning a cruise operation and a discrete 1-cosine gust are implemented. The gust load illustration is depicted in Figure 6. Based on FAR 25, the interval of gust gradient H_g between 30 feet (9 m) and 350 feet (107 m) can be evaluated with a typical distance of 12.5 average aerodynamic chords (MAC). For benchmark, an extreme 15 m/s maximum gust speed amplitude, V_{g0}, is applied.

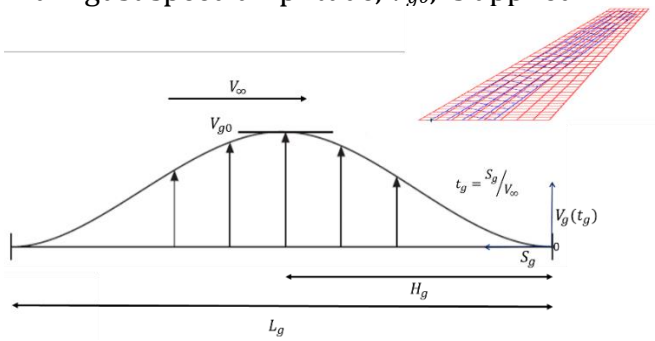

Figure 6 Illustration of a discrete 1-Cosine gust

As provided on Figure 7, it is seen that the smallest gust distance exerts the lowest deflection amplitude. On the other hand, the 12.5 MAC (43 m) gust load distance delivers the highest deflection amplitude. The disturbance only has a short 75 milliseconds time to exert influence on the structure when H_g = 9 meters. In the contrary, the gust load impales the wing design near 1 second, inducing a slow vertical speed response when H_g = 107 m. In this load case, the transient influence is lower than other phenomenons. Conversely, when H_g is 12.5 times MAC, the perturbation withstands enough value to induce the highest amplitude. It maintains a fast vertical speed structural response and shows further damped vibrations even after the gust is finished. Therefore, the value of H_g = 12.5 MAC is used in this work.

Figure 8 provides the electric potential outputs at different iteration steps. The optimum resistance load value is used. It is observed that the responses of all stages of iteration are almost indistinguishable. When zoomed in, the first iteration marked by the dashed pink curve overestimates both further iterations slightly. Further discussed, the response decreases at the second iteration, and increases slightly once more on the last iteration.

For further discussion, Table 1 shows the iterative procedure from a harvested energy perspective. The variance from the first to the next iteration is only about 5%, and the difference after the last iteration is less than 1%. The energy value converges at around 2.49 kJ. In this occasion, the structural displacement is not dominantly influenced by the mechanical load, hence the structural deformation is also not significantly affected by the feedback piezoelectric effect.

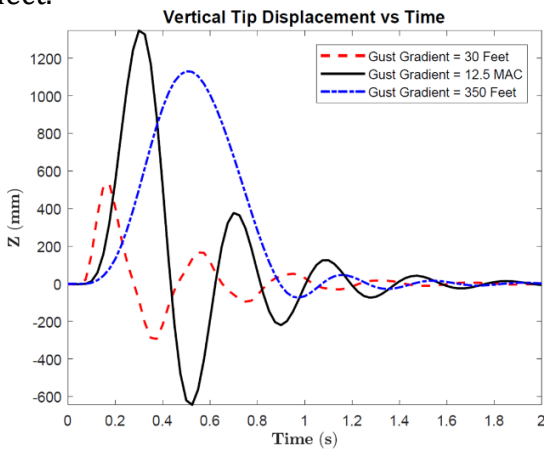

Figure 7 The vertical tip displacement time response with V_{g0} =15 m/s and various H_g

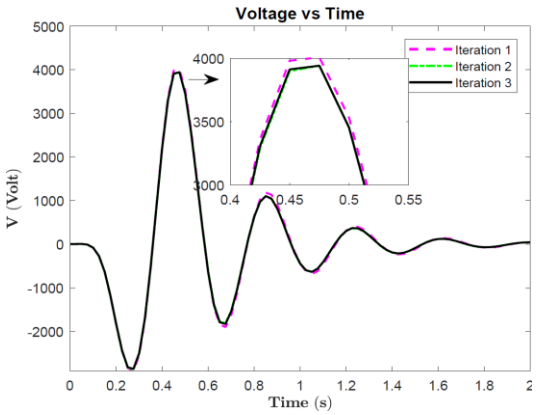

Figure 8 The electric potential output time history with H_g equals 12.5 times MAC at various steps of iteration

Table 1 Electrical energy output of the aircraft wing on each iteration step

Iteration Step	Energy Harvested (kJ)	Variance n^{th} step – $(n-1)^{th}$ step
1	2.609	-
2	2.475	5.14 %
3	2.499	0.97 %
4	2.488	0.43 %
5	2.492	0.15 %

The stress and failure analysis of the structure due to the flying state and the collected electrical power are undertaken for the first time in this work, which concerns the structural strength. As a result of the suggested iterative FEM's ease of use in commercial software, numerous numerical analysis tools can be used to enable the observation of energy harvesting structures. The gust and failure analysis numerical modules from commercial software can be used simultaneously in this situation, allowing the failure index of the wing equipped with active energy harvesting to be explored when subjected to gust loading.

Based on the computed stress contour, the tension on the lower skin and compression on the upper skin are observable. At the same time, the wing is deformed upward due to the aerodynamics load. The stress concentration is observed on the lower skin located at trailing edge close by the wing root. As illustrated on Figure 9, The maximum stress doubles from V_g = 15 m/s. The yield strengths of the materials, Al-2219 and PZT-5A are 352 MPa (Matweb, 2001), and 140 MPa (Anton et al., 2012), respectively. Therefore, the stress is still within the linear elastic regime.

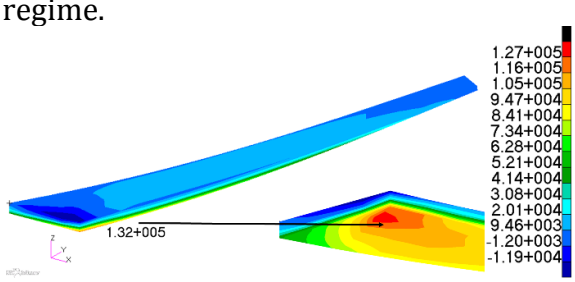

Figure 9 Stress distribution, Case with V_{g0} = 15 m/s and H_g = 12.5 x MAC on t_g = 0.3 seconds (stress unit in kPa)

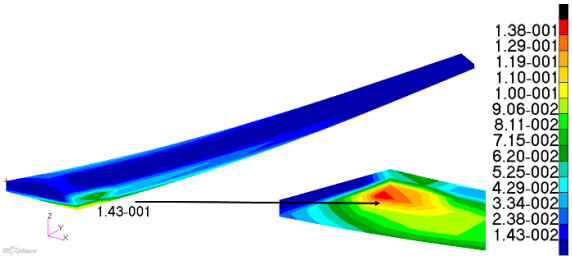

Figure 10 Failure indices, Case with V_{g0} = 15 m/s and H_g = 12.5 x MAC at t_g = 0.3 seconds

Tsai-Wu theory is utilized for the wing structure failure analysis. The failure index is set to 0-1 in this case. The materials' yield and tensile strengths are being considered. Taking as a note, the PZT-5A has brittle characteristic; thus, the yield strengths is equal to the tensile forces. The zero (0) and one (1) indexes, respectively, denote no damage to the structure and a total failure.

Figure 10 depicts that the maximum failure index is 0.14. As a result, even in extreme conditions such as 15 m/s gust amplitude, the wing structure is considered safe.

Furthermore, because the failure indices at the upper skin are less than 0.1, the piezoelectric layer is safe.

According to the data in Engineering Sciences Data Unit (ESDU) for gust load chances, a 15 m/s amplitude is considered high and rarely happens in typical flight conditions. A 15 m/s gust speed has a 0.1 percent chance of occurring at a flying altitude of 10 km. Hence, the output shown in Table 1 could be considered only as am upper benchmark. Gust amplitudes of 5 m/s and 10 m/s were evaluated concerning more realistic settings. To be clear, ESDU's data are reported in Equivalent Air Speed (EAS), which is an equivalent speed with sea level dynamic pressure. As a result, 5 m/s, 10 m/s, and 15 m/s gust speeds are roughly 3 m/s, 6 m/s, and 9 m/s, in EAS, respectively.

As discussed in (Akbar & Curiel-Sosa, 2018), the implementation of multiphase composite could provide a better weight-energy trade-off in comparison to the one with pure piezoelectric material. Hence, for further evaluation, a multiphase, double inclusion piezoelectric/carbon fiber with 50 percent and 0.2 in aspect ratio is used to replace PZT-5A at the upper skin.

Figure 11 shows the multiphase composites' electric potential and power responses for various gust amplitudes. As expected, the smaller the gust amplitude, the lower the voltage and power output. The gust amplitude of 3, 6, and 9 m/s EAS yields electrical energies of 0.28, 1.13, and 2.39 kJ, respectively. The comparison of the maximum power generated is shown in Table 2 and it is seen that present work's underestimate the earlier work's results. The previous work by Akbar and Curiel-Sosa in (2018) undertook the assumption of harmonically oscillating cruise lifting load. In practicality, their belief may only occur in a rare circumstance, i.e., extremely high amplitude and continuous gust disturbance.

Table 2 Comparison of the maximum power of the aircraft wing for different load cases

	Load Case	Maximum Power (kW)
Present work	1-Cosine Gust (3 m/s EAS Amplitude)	1.8
	1-Cosine Gust (6 m/s EAS Amplitude)	7.3
	1-Cosine Gust (9 m/s EAS Amplitude)	15.5
Earlier work (Akbar and Curiel-Sosa, 2018)	Harmonic cruise lift with ecitation at near the 1st bending frequency	41.8

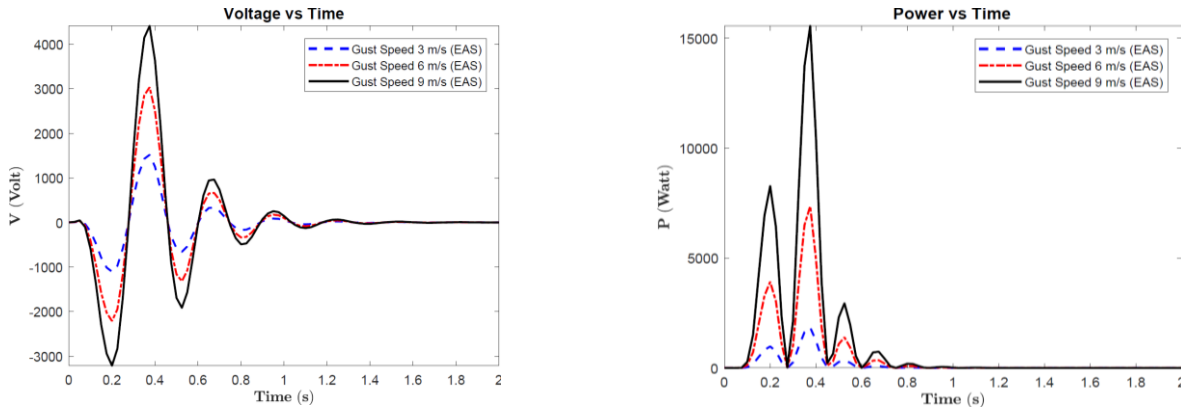

(a) (b)

Figure 11 The transient responses of (a) output voltage and (b) output power on the wing structures with multiphase composite for various gust amplitudes (Up gust) at H_g = 12.5 MAC

Referring to the data published by ESDU, at a specific amplitude, down-gust, which vector points out to a downward direction may also occur. According to Figure 12, the

down-gust response is identical to the previously analyzed up-gust response, with the only significant change being the voltage direction.

At a flight altitude of 10000 meters, the average distance flown to meet an up- or down-gust is roughly 5200 km or 2800 nautical miles for a cloud warning radar-equipped aircraft. This distance is similar to a long-range aircraft flying at 240 m/s for 6 hours of cruise endurance (total flight in 7 to 8 hours). At this height, the ratio between down-gust to up-gust is roughly one; consequently, there is an equal risk of encountering a down-gust or an up-gust.

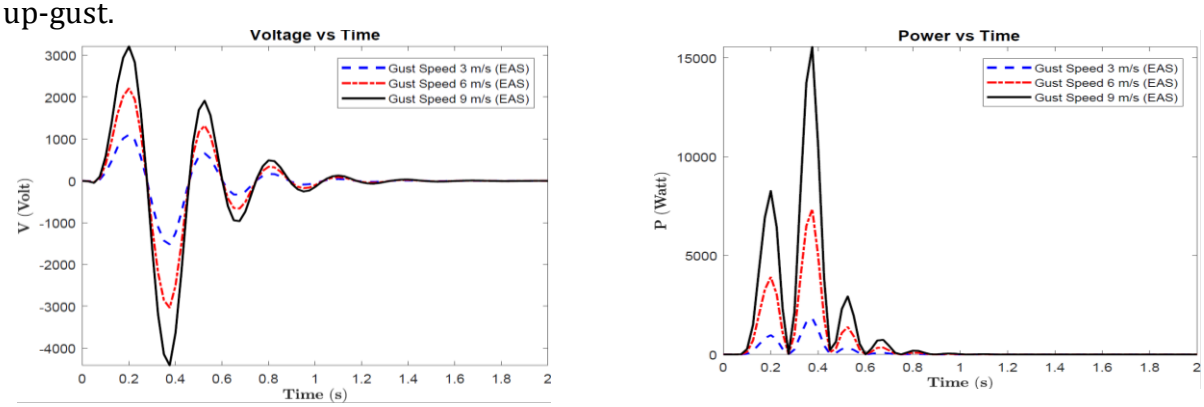

(a) (b)

Figure 12 The transient responses of (a) output voltage and (b) output power on the wing structures with multiphase composite for various gust amplitudes (Down gust) at H_g = 12.5 MAC

A gust occurrence chance is unique for a given gust amplitude. Based on ESDU, the probabilities of gust with 5 m/s, 10 m/s, and 15 m/s amplitudes (which in EAS 3 m/s, 6m/s, and 15 m/s, respectively) are 10%, 3%, and 0.1%, respectively. Thus, the gust at 5 m/s amplitude example is the most realistic among the three gust amplitudes evaluated.

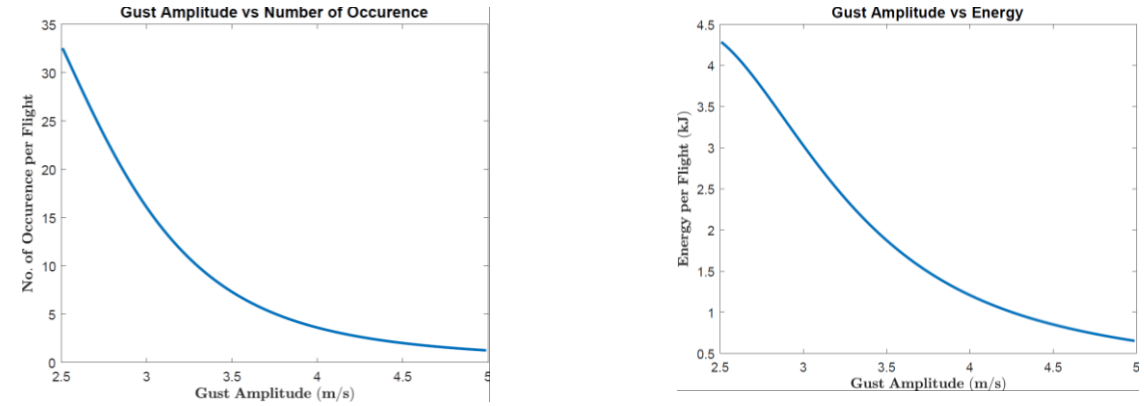

(a) (b)

Figure 13 (a) The gust amplitude occurrence for each flight, and (b) Total produced energy as a function of gust amplitude V_g for each flight

As both wings generate the energy, then using a 5 m/s of gust only could yield around 0.56 kJ harvested energy. Besides, concerning lower amplitude gusts, it is also more likely that the gust could occur more than once. Figure 13a shows the chance of smaller gust amplitude happening based on the data from ESDU. The lowest gust amplitude of 2.5 m/s was found to occur more than 30 occurrences every flight.

Figure 13b depicts the relationship between total generated energy per flight and gust amplitude. It turns out that a smaller gust amplitude does not always imply a lower amount of energy harvested during the flight, as a smaller gust amplitude can lead to a higher

number of interactions. As a result, each flight may yield a higher total gathered energy. Despite this, the maximum energy captured per flight (based on 2.5 m/s gust) is just around 4.3 kJ. When compared to the fuel-energy ratio of an Auxiliary Power Unit (1200 kJ per pound of fuel), this amount of energy is still on a lower scale. Hence, the flight performance improvement, such as extended flight range will be insignificant or even negligible. In addition, the highlight of the aircraft and wing configurations, flight operating conditions, and energy harvesting parameters are given in Table 3.

Table 3 Configuration, operation, and energy harvesting parameters highlight

Aircraft class	Wing configuration	Harvesting Structure	Flight Condition	Gust Load	Gust Chance	Energy Harvested
Typical long-range jet transport aircraft (7-8 hours flight)	Sweptback wing with 13.9 m half-span and 3.5 m mean chord	Multiphase composite with carbon fiber-PZT 5A double inclusion core	Cruise flight at 10 km altitude with gust wind loading	1-Cosine gust with amplitude of 2.5 m/s and 86 m gust length	30-33 encounters per flight	4.3 kJ per flight

4. Conclusions

The iterative FEM scheme implementation provides a more realistic flight loading approach to the wing structure of a jet transport airplane imposed by cruise load and gust disturbance. The analyses discussed in this paper have integrated the aeroelastic aspects with structural dynamic and unsteady aerodynamic numerical model. The use of commercial software in iterative FEM has allowed for the evaluation of numerous forms of structural analyses, such as gust and failure modules. The stress and failure studies of the wing, when subjected to the gust load and harvesting the energy, were undertaken in this work. The wingbox is safe even when confronting a high wind while generating the electrical power, according to the failure study. Thus, the multidisciplinary problem concerning structural strength, aeroelastic vibration, and energy harvesting, can be solved with this iterative FEM scheme. This study depicted a more practical result by utilizing a more realistic load model for gust and cruise loads. The gust's response pointed out that structural vibration was quickly damped during a cruise flight; thus, the maximum gathered power being attained in a relatively short time. Furthermore, a significant amplitude gust may only occur once at a given distance, preventing continuous power harvesting via structural vibration owing to aeroelastic gust throughout a typical flight. According to the data presented in this paper, the energy captured during a typical cruise flight under gust perturbation is likely low compared to the energy delivered by the aircraft system, such as the Auxiliary Power Unit. Therefore, the piezoelectric energy harvesting structure is not feasible to support the aircraft's main power supply. The gathered energy, on the other hand, might be utilized to improve the efficiency of other aircraft systems, i.e., active disturbance control, such as a gust alleviation system.

Acknowledgements

The authors would like to thank Mr. Nanda Wirawan (National Research and Innovation Agency of Indonesia) for his assistance with the computational work. We also appreciate the support offered by the ITB Research, Community Service, and Innovation Program (P2MI ITB) under grant no. 2C/IT1.C04/SK/KP/2021.

References

Abdelkefi, A., 2016. Aeroelastic Energy Harvesting: a Review. *International Journal of Engineering Science*, Volume 100, pp. 112–135

Ainsworth, J., Collier, C., Yarrington, P., Lucking, R., Locke, J., 2010. Airframe Wingbox Preliminary Design and Weight Prediction. *In*: 69th International Conference on Mass Properties, Virginia Beach, Virginia, pp. 155–195

Akbar, M., Curiel-Sosa, J.L., 2016. Piezoelectric Energy Harvester Composite under Dynamic Bending with Implementation to Aircraft Wingbox Structure. *Composite Structures*, Volume 153, pp. 193–203

Akbar, M., Curiel-Sosa, J.L., 2018. Implementation of Multiphase Piezoelectric Composites Energy Harvester on Aircraft Wingbox Structure with Fuel Saving Evaluation. *Composite Structures*, Volume 202, pp. 1000–1020

Akbar, M., Curiel-Sosa, J.L., 2019. An Iterative Finite Element Method for Piezoelectric Energy Harvesting Composite with Implementation to Lifting Structures under Gust Load Conditions. *Composite Structures*, Volume 219, pp. 97–110

Anton, S.R., Erturk, A., Inman, D.J., 2012. Bending Strength of Piezoelectric Ceramics and Single Crystals for Multifunctional Load-Bearing Applications. *IEEE Transactions on Ultrasonics Ferroelectronics and Frequency Control*, Volume 59(6), pp. 1085–1092

Anton, S.R., Inman, D.J., 2008. Vibration Energy Harvesting for Unmanned Aerial Vehicles. *In*: Proceeding of SPIE-Active and Passive Smart Structures Integrated Systems, Volume 6928, p. 692824

Anton, S.R., Sodano, H.A., 2007. A Review of Power Harvesting using Piezoelectric Materials (2003-2006). *Smart Materials and Structures*, Volume 16(3), pp. 1–21

Brazovskaia, V., Gutman, S., 2021. Classification of Regions by Climatic Characteristics for the Use of Renewable Energy Sources. *International Journal of Technology*, Volume 12(7), pp. 1537–1545

Bruni, C., Gibert, J., Frulla, G., Cestino, E., Marzocca, P., 2017. Energy Harvesting from Aeroelastic Vibrations Induced by Discrete Gust Loads. *Journal of Intelligent Material Systems and Structures*, Volume 28(1), pp. 47–62

Cheng, Y, Li, D., Xiang, J., Ronch, A.D., 2019. Energy Harvesting Performance of Plate Wing from Discrete Gust Excitation. *Aerospace*, Volume 6(3), pp. 37–49

Christodoulou, L., Venables, J.D., 2003. Multifunctional Material Systems: the First Generation. *JOM: the journal of the Minerals Metals & Materials Society,* Volume 55(12), pp. 39–45.

De-Marqui, J.C., Erturk, A., Inman, D.J., 2009. An Electromechanical Finite Element Model for Piezoelectric Energy Harvester Plates. *Journal of Sound and Vibration*, Volume 327(1), pp. 9–25

De-Marqui, J.C., Erturk, A., Inman, D.J., 2010. Piezoaeroelastic Modeling and Analysis of a Generator Wing with Continuous and Segmented Electrodes. *Journal Intelligent Material Systems and Structures*, Volume 21(10), pp. 983–993

De-Marqui, J.C., Vieira, W.G.R., Erturk, A., Inman, D.J., 2011. Modeling and Analysis of Piezoelectric Energy Harvesting from Aeroelastic Vibrations using the Doublet-Lattice Method. *Journal of Vibration and Acoustics*, Volume 133(1), p. 011003

Erturk, A., Vieira, W.G.R., De-Marqui, J.C., Inman, D.J., 2010. On the Energy Harvesting Potential of Piezoaeroelastic Systems. *Applied Physics Letters*, Volume 96(18), p. 184103

Ferreira, A.D.B.L., Nóvoa, P.R.O., Marques, A.T., 2016. Multifunctional Material Systems: A State-of-the-Art Review. *Composite Structures*, Volume 151, pp. 3–35

Guenther, M., 2018. Challenges of a 100% Renewable Energy Supply in the Java-Bali Grid.

International Journal of Technology, Volume 9(2), pp. 257–266

Hafizh, H., Hamsan, R., Zamri, A.A.A., Keprawi, M.F.M., Hiromichi, S., 2018. Solar Updraft Power Generator with Radial and Curved Vanes. *In*: AIP Conference Proceeding, Volume 1930(1), p. 020018

Krasniqi, G., Dimitrieska, C., Lajqi, S., 2022. Wind Energy Potential in Urban Area: Case study Prishtina. *International Journal of Technology*, Volume 13(3), pp. 458–472

Li, D., Wu, Y., Ronch, A.D., Xiang, J., 2016. Energy Harvesting by Means of Flow-Induced Vibrations on Aerospace Vehicles. *Progress in Aerospace Sciences*, Volume 86, pp. 28–62

Matweb, 2001. *Aluminum 2219-Material Data*. Available online at http://www.matweb.com/, Accessed on December 2021

Rostami, A.B., Armandei, M., 2017. Renewable Energy Harvesting by Vortex-Induced Motions: Review and Benchmarking of Technologies. *Renewable and Sustainable Energy Reviews*, Volume 70, pp. 193–214

Sairajan, K.K., Aglietti, G.S., Mani, K.M., 2016. A Review of Multifunctional Structure Technology for Aerospace Applications. *Acta Astronautica*, Volume 120, pp. 30–42

Saporito, M., Da-Ronch, A., 2020. Aeroelastic Energy Harvesting from Statistically Representative Gust Encounters. *Journal of Fluids and Structures*, Volume 94, p. 102869

Selvan, K.V., Ali, M.S.M., 2016. Micro-Scale Energy Harvesting Devices: Review of Methodological Performances in the Last Decade. *Renewable and Sustainable Energy Reviews*, Volume 54, pp. 1035–1047

Thomas, J.P., Qidwai, M.A., Kellogg, J.C., 2006. Energy Scavenging for Small-Scale Unmanned Systems. *Journal of Power Sources*, Volume 159(2), pp. 1494–1509

Tsushima, N., Su, W., 2016. Modeling of Highly Flexible Multifunctional Wings for Energy Harvesting. *Journal of Aircraft*, Volume 53(4), pp. 1033–1044

Tsushima, N., Su, W., 2017. Concurrent Active Piezoelectric Control and Energy Harvesting of Highly Flexible Multifunctional Wings. *Journal of Aircraft*, Volume 54(2), pp. 724–736

Xiang, J., Wu, Y., Li, D., 2015. Energy Harvesting from the Discrete Gust Response of a Piezoaeroelastic Wing: Modeling and Performance Evaluation. *Journal of Sound Vibration*, Volume 343, pp. 176–193